Heat transport in stagnant lid convection with temperature-and pressure-dependent Newtonian or non-Newtonian rheology

Caroline Dumoulin, Marie-Pierre Doin, Luce Fleitout

JOURNAL OF GEOPHYSICAL RESEARCH, VOL. 104, NO. B6, PAGES 12,759–12,777, JUNE 10, 1999

Heat transport in stagnant lid convection with temperature- and pressure-dependent Newtonian or non-Newtonian rheology

Caroline Dumoulin, Marie-Pierre Doin, and Luce Fleitout

Laboratoire de Géologie, CNRS, URA 1316, Ecole Normale Supérieure, Paris

Abstract. A numerical model of two-dimensional Rayleigh-Bénard convection is used to study the relationship between the surface heat flow (or Nusselt number) and the viscosity at the base of the lithosphere. Newtonian or non-Newtonian, temperature- and pressure-dependent rheologies are considered. In the high Rayleigh number time-dependent regime, calculations yield $Nu \propto Ra_{BL}^{1/3} b_{eff}^{-4/3}$, where b_{eff} is the effective dependence of viscosity with temperature at the base of the upper thermal boundary layer and Ra_{BL} is the Rayleigh number calculated with the viscosity ν_{BL} (or the effective viscosity) at the base of the upper thermal boundary layer. The heat flow is the same for Newtonian and non-Newtonian rheologies if the activation energy in the non-Newtonian case is twice the activation energy in the Newtonian case. In this chaotic regime the heat transfer appears to be controlled by secondary instabilities developing in thermal boundary layers. These thermals are advected along the large-scale flow. The above relationship is not valid at low heat flow where a stationary regime prevails and for simulations forced into steady state. In these cases the Nusselt number follows a trend $Nu \propto Ra_{BL}^{1/5} b_{eff}^{-1}$ for a Newtonian rheology, as predicted by the boundary layer theory. We argue that the equilibrium lithospheric thickness beneath old oceans or continents is controlled by the development of thermals detaching from the thermal boundary layers. Assuming this, we can estimate the viscosity at the base of the stable oceanic lithosphere. If the contribution of secondary convection to the surface heat flux amounts to 40 to 50 mW m^{-2}, the asthenospheric viscosity is predicted to be between 10^{18} and 2×10^{19} Pa s.

1. Introduction

A heat supply at the base of the lithospheric plates seems necessary to explain the equilibrium thickness of the oceanic and continental lithospheres and the flattening of the seafloor at old ages [e.g., *Doin and Fleitout*, 1996; *Parsons and Sclater*, 1977]. Secondary convection can be a good explanation for this heat source [*Fleitout and Yuen*, 1984a]. Here we present a parameterization of the heat carried by secondary convection using a temperature- and pressure-dependent, Newtonian or non-Newtonian rheology.

In the past, scaling relations for the heat transport in Rayleigh-Bénard settings (heated from below) at large or infinite Prandtl numbers have been theoretically, numerically, and experimentally studied, for isoviscous or temperature-dependent viscosity fluids.

Paper number 1999JB900110.
0148-0227/99/1999JB900110$09.00

For isoviscous stationary flows, the asymptotic boundary layer theory predicts a relationship between the Nusselt number Nu and the Rayleigh number Ra, yielding either $Nu \propto Ra^{1/3}$ for free slip boundary conditions [*Turcotte and Oxburgh*, 1967], or $Nu \propto Ra^{1/5}$ for rigid boundary conditions [*Roberts*, 1979]. Numerous theories proposed various scaling relations for turbulent isoviscous flows which prevail at high Ra. The mixing length theory [*Kraichnan*, 1962] and the boundary layer stability analysis [*Howard*, 1964] both yield $Nu \propto Ra^{1/3}$. For rigid boundary conditions, the slope β in $Nu \propto Ra^{\beta}$ is therefore predicted to increase from stationary to turbulent flows. Indeed, analogical experiments with high Prandtl numbers (greater than 30) and high Rayleigh numbers yield values of β around 0.283 [e.g., *Somerscales and Gazda*, 1968] or 1/3 [e.g., *Dropkin and Somerscales*, 1965; *Goldstein et al.*, 1990], whereas steady state numerical experiments yield lower values of β, around 0.223 [*Deschamps*, 1997; *Frick et al.*, 1983], closer to the asymptotic boundary layer prediction. For free slip boundary conditions, predicted slopes are the same for stationary and high Rayleigh number flows.

Thus steady state numerical experiments from *Christensen* [1984a], *Deschamps* [1997], *Jarvis and Peltier* [1982], and *Schubert and Anderson* [1985] yield β close to 0.32, in good agreement with the asymptotic boundary layer theory [*Olson*, 1987]. By comparison, turbulent time-dependent convection shows a similar exponent $\beta = 0.315$ [*Hansen et al.*, 1992].

For a strongly temperature-dependent viscosity, the Rayleigh number has been defined either with the viscosity horizontally averaged at the top boundary [e.g., *Booker*, 1976; *Christensen*, 1989] or at the middle height of the box [e.g., *Christensen*, 1984b; *Larsen et al.*, 1995], or calculated for the averaged temperature of the box [e.g., *Nataf and Richter*, 1982] (see Figure 1). This choice strongly affects the Nu versus Ra parameterization [*Christensen*, 1985]. However, neither choice is really adapted to the parameterization with rigid lid boundary condition. *Honda* [1996] showed the usefulness of the locally defined Ra and Nu for a convection with temperature-dependent viscosity. *Morris and Canright* [1984] and *Davaille and Jaupart* [1993] introduced an effective temperature drop δT_{eff} which drives the convection, proportional to $\delta T_\nu = (-\partial \ln \nu / \partial T)^{-1} = b^{-1}$ where b is the dimensionless temperature dependence of the viscosity. *Davaille and Jaupart* [1993], for transient cooling experiments, and *Grasset and Parmentier* [1998], for numerical simulations of a fluid heated from within, showed that $\delta T_{\text{eff}} = 2.23 b^{-1}$. In the rigid lid regime, the asymptotic boundary layer analysis leads to $Nu \propto b^{-1} Ra_i^{1/5}$ where Ra_i is the Rayleigh number defined by the viscosity in the interior of the cell [*Fowler*, 1985]. This relationship is verified by numerical experiments resulting in stationary flows [*Moresi and Solomatov*, 1995]. However, analogical experiments give $Nu \propto b^{-4/3} Ra_i^{1/3}$ [*Davaille and Jaupart*, 1993], in good agreement with the boundary layer stability analysis first developed by *Howard* [1964]. *Howard* [1964] assumed that boundary layers are in a marginal stability state maintained by a cyclic process: Thermals detach occasionally from the thermal boundary layers when the Rayleigh number defined locally at the base of the lithosphere grows beyond the critical Rayleigh number. This analysis yields $Nu = (Ra_i / Ra_{\text{cr}})^{1/3}$. For a viscosity depending exponentially on temperature, $Ra_{\text{cr}} \propto b^4$ [see *Stengel et al.*, 1982], one gets $Nu \propto Ra_i^{1/3} b^{-4/3}$ [*Solomatov*, 1995].

Only a few studies have been done on parameterizations with temperature- and pressure-dependent viscosity. Simulations with a rigid upper boundary of *Fleitout and Yuen* [1984b] and with a moving upper boundary of *Doin et al.* [1997] show that the surface Nusselt number varies with the viscosity at the base of the lithosphere and is not directly sensitive to the viscosity pressure dependence. *Doin et al.* [1997] have also shown that the presence of primary convection does not strongly affect the heat transport through the base of the lithosphere. Therefore we shall analyze the relation between the surface Nusselt number and the viscosity at the base of the upper thermal boundary layer (UTBL) for a fixed upper boundary.

For fluids with "isoviscous" Newtonian and non-Newtonian rheologies, the Nu versus Ra relationship does not depend on the stress exponent n, provided that the Rayleigh number is defined with a judiciously chosen effective viscosity [*Parmentier and Morgan*, 1982; *Parmentier et al.*, 1976]. *Christensen* [1984a] and *Cserepes* [1982] compared the patterns of the steady state flows for temperature-dependent non-Newtonian and Newtonian rheologies. *Christensen* [1984a] shows that the characteristics of steady state flows are similar if one divides the activation energy and volume for the non-Newtonian rheology by 2 or 3. However, in time-dependent simulations, the temporal variability of the flow is highly increased in the non-Newtonian rheology [e.g., *Christensen and Yuen*, 1989; *Fleitout and Yuen*, 1984a; *Larsen et al.*, 1997].

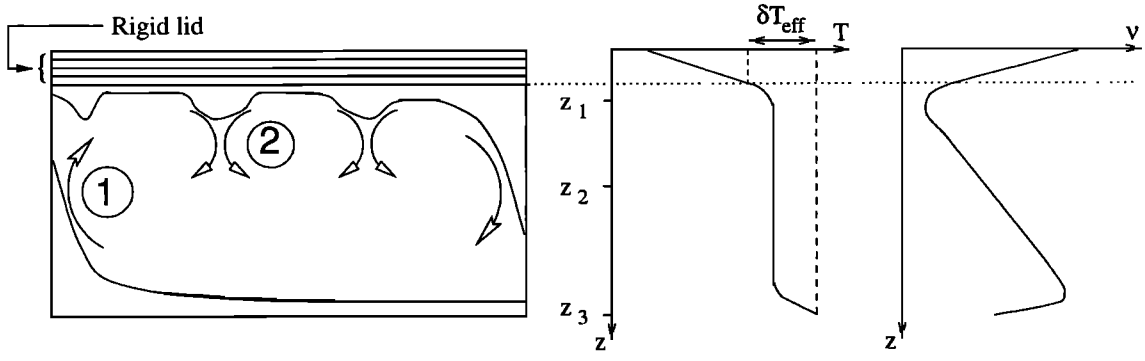

Figure 1. When the viscosity strongly depends on temperature, a conductive rigid lid develops at the top of the box. The temperature drop below the lid is then reduced to δT_{eff}. The viscosity (ν) and temperature (T) used to define the Rayleigh number, can be evaluated either at depth z_1 (base of the lithosphere), or at z_2 (middepth) or at z_3 (bottom of the box). Process 1 illustrates large-scale stationary convection as has been described theoretically by *Fowler* [1985]. Process 2 illustrates small-scale destabilization of the lid as has been observed *Davaille and Jaupart*'s [1993] experiments and described theoretically by *Solomatov* [1995].

In the present work, the rheologies used are Newtonian or non-Newtonian with temperature- and pressure-dependent viscosity. A wide range of Rayleigh numbers (defined with the viscosity at the base of the lithosphere) is explored and, therefore, the obtained results go from a steady state to a "chaotic " regime: The scaling laws for the heat transport for the two regimes are searched for. The Rayleigh number exponent is looked at, from the stationary regime to the turbulent regime, in order to explain when the different predictions of the asymptotic boundary layer theory and the boundary layer stability analysis apply. Another purpose is to include the effect of the pressure dependence of viscosity in the parameterization. At last, we explore a parameterization in the non-Newtonian case, an attempt which has never been done so far on the basis of numerical experiments.

2. Model and Boundary Conditions

The convection code built by *Christensen* [1983, 1984a] is used in this study. We consider a two-dimensional convection in a Boussinesq fluid with an infinite Prandtl number which is heated from below. The code solves the equations of conservation of mass, energy, and momentum. We neglect internal heating and viscous dissipation. Calculations are dimensionless. The temperature is fixed at the bottom ($T_B = 1$) and at the top ($T_T = 0$). To insure that the heat transfer rate is representative of the rigid lid regime, we choose high viscosity contrasts and a no-slip boundary condition at the top of the box. Other boundary conditions on the bottom and sides of the box are free slip. We assume that the strain rate $\dot{\varepsilon}_{ij}$ depends on the deviatoric stress σ_{ij} according to

$$\dot{\varepsilon}_{ij} = A^{-1}\sigma_{\mathrm{II}}^{n-1}\sigma_{ij}\exp(bT - cz) \tag{1}$$

where $n = 1$ for diffusion creep and $n = 3$ for dislocation creep, A is a constant, b and c are, respectively, the coefficients characterizing the nondimensional temperature and depth dependence of viscosity, and σ_{II} is the second invariant of the stress tensor. The effective viscosity is written as follows:

$$\nu^*_{\mathrm{eff}} = A^{1/n}\dot{\varepsilon}_{\mathrm{II}}^{-(1-\frac{1}{n})}\exp(-\frac{b}{n}T + \frac{c}{n}z) \tag{2}$$

where $\dot{\varepsilon}_{\mathrm{II}}$ is the second invariant of the strain tensor. The nondimensional effective viscosity is

$$\nu_{\mathrm{eff}} = A^{-\frac{1}{n}}\nu^*_{\mathrm{eff}}\left(\frac{H^2}{K}\right)^{-[1-(\frac{1}{n})]} \tag{3}$$

where K is the thermal diffusivity and H the height of the box. The (effective) viscosity characterizing convection is here defined at the base of the lithosphere. In the case of a Newtonian rheology, the dimensionless viscosity at the base of the lithosphere is given by $\nu_{\mathrm{BL}} = \exp(-bT_i + cz_{\mathrm{BL}})$ where T_i is the horizontally averaged temperature at middepth and z_{BL} is the thickness of the lithosphere ($z_{\mathrm{BL}} = T_i/Nu$, assuming that the temperature gradient is constant in the lithosphere, where Nu is the surface Nusselt number). In the case of non-Newtonian rheology, $\nu_{\text{eff-BL}}$ is the minimum of the horizontal mean of the logarithm of the effective viscosity for the box (except for $c = 0$, where $\nu_{\text{eff-BL}}$ is evaluated at $z = \frac{1}{2}(z_{\max} + z_{\mathrm{BL}})$, where $z_{\max}$ is the depth of the local maximum of temperature beneath the UTBL).

Various definitions of the Rayleigh number are used. In the Newtonian case we define $Ra_{\mathrm{BL}-N}$ as

$$Ra_{\mathrm{BL}-N} = \frac{\alpha\rho g\Delta T H^3}{K\nu^*_{\mathrm{BL}}} = Ra_0\nu^{-1}_{\mathrm{BL}} \tag{4}$$

where α is thermal expansion coefficient, ρ is the density, g is the gravity acceleration, ΔT is the temperature drop across the box, ν^*_{BL} is the viscosity at the base of the lithosphere, and Ra_0 is the Rayleigh number calculated with the surface viscosity A. For the non-Newtonian rheology, two different Rayleigh numbers are defined. The effective Rayleigh number at the base of the lithosphere, which can be compared to $Ra_{\mathrm{BL}-N}$, is written as follows:

$$Ra_{\text{BL-eff}} = \frac{\alpha\rho g\Delta T H^3}{K\nu^*_{\text{eff-BL}}} = Ra_0\nu^{-1}_{\text{eff-BL}} \tag{5}$$

where $\nu_{\text{eff-BL}}$ is the effective viscosity at the base of the lithosphere. However, the only free parameter is the non-Newtonian Rayleigh number ($n = 3$). It is evaluated with the viscosity at the base of the lithosphere:

$$\begin{aligned} Ra_{\text{BL-nN}} &= \frac{\alpha\rho g\Delta T H^{5/3}}{K^{1/3}A^{1/3}\exp(-\frac{b}{3}T_i + \frac{c}{3}z_{\mathrm{BL}})} \\ &= Ra_0\exp(\frac{b}{3}T_i - \frac{c}{3}z_{\mathrm{BL}}) \end{aligned} \tag{6}$$

Most calculations are time-dependent but, for some others, the flow is forced toward a steady state (time dependence is not allowed, time variations are strongly damped using an underrelaxation factor larger than 0.75). For time-dependent calculations the box is divided into 121×25 cells and has an aspect ratio of 4. The spacing of the grid is uniform in the horizontal direction, while in the vertical direction the grid is denser at the base of the lithosphere and in the hot thermal boundary layer in order to increase the accuracy. For steady state calculations the box is divided into 70×60 or into 100×60 cells and has an aspect ratio of 1 for Newtonian rheology and of 2 for non-Newtonian rheology. To estimate the accuracy on Nu and Ra_{BL} obtained with numerical simulations, a convergence test is performed in the time-dependent case of Newtonian rheology, $Ra_0 = 9900$, $b = 13.0$, and $c = 4.2$ (see Table 1). It shows that when the vertical grid is of 25 points and refined in active boundary layers, the obtained Nu and Ra_{BL} values are very close to those obtained with a 61 vertical grid with a regular spacing. The compari-

Table 1. Convergence Test Done in Newtonian Rheology for $Ra_0 = 9900$, $b = 13.0$, and $c = 4.2$

Grid (Aspect Ratio of 4)	Nu	$Ra_{\text{BL-N}}$
121×21[a]	9.20	1.78×10^8
121×41[a]	9.62	1.61×10^8
121×61[a]	9.54	1.53×10^8
181×37[b]	9.49	1.69×10^8
241×37[b]	9.41	1.66×10^8
121×25[b,c]	9.56	1.55×10^8

[a]Uniform grid spacing vertically.
[b]Vertical grid denser at the base of the lithosphere.
[c]Grid used for the result presented in this study.

son of the results with a 121×25 grid and with a 241×37 grid (both refined on thermal boundary layers) yields a rough error estimate of 0.15 for Nu (1.5%) and of 8% for Ra_{BL} (3% for $Ra_{\text{BL}}^{1/3}$).

Our purpose is to relate the surface Nusselt number to the effective viscosity at the base of the lithosphere. The results of time-dependent and steady state calculations are given in Tables 2 and 3. In these tables, b and c are the coefficients characterizing the dimensionless temperature and depth dependence of the viscosity, $\dot{\varepsilon}_{\text{max}}$ is the maximum value of the strain rate, and v_{RMS} is the RMS of the velocity vector. The standard deviation of Nu, σ_{Nu}, measures the variability of Nu with time. The numerical error on Nu (~0.15) plus the noise due to limited time averaging of chaotic fluctuations (< 0.20) is therefore less than 0.35.

3. Description of the Flow for Time-Dependent Calculations

For time-dependent calculations and for small Rayleigh numbers, a real steady state is obtained, for both Newtonian and non-Newtonian rheologies: Each variable reaches a constant value and remains stable. Small-scale instabilities are not observed. We obtain four large symmetrical convective cells in the case of Newtonian rheology (see Figure 2a) and two in the case of non-Newtonian rheology.

On the other hand, for high Rayleigh numbers, the convection becomes highly time-dependent. A statistically stationary regime is reached, when time averages of variables (such as the internal temperature and the surface and bottom heat flows) have reached an asymptotic value independent of time. At this stage of quasi-equilibrium, the mean surface heat flow is equal to the mean bottom heat flow. In chaotic states, cyclic variations both at short and intermediate timescales are noticeable in the temporal evolution of heat flux, temperature, viscosity, etc. For the non-Newtonian rheology, the relative amplitude of the short-term variations can reach 10% for the surface heat flow and 3% for the internal temperature (see Figure 3). In Figure 4 the surface heat flow and the effective viscosity at the bottom of the UTBL, $\nu_{\text{eff-BL}}$, are low-pass filtered to eliminate short-term variations by a convolution with a Gaussian function. The width of the Gaussian function depends on the frequency of the short-term variations (the width is about 10 times the periods of short-term variations). At intermediate timescales, cyclic variations of the Nusselt number as a function of ν_{BL} around an average point (Nu,ν_{BL}) are also observed (see Figure 4). In the Newtonian case the variations have a smaller amplitude.

The pattern of convection in these simulations and the power spectrum of the flow are similar to those of isoviscous turbulent flows [*Hansen et al.*, 1990]. Instabilities or thermals are generated at the base of the stagnant lid and at the bottom thermal boundary layer (see Figure 2b). These instabilities are carried away by a large-scale circulation. Thermals are advected toward main downwellings or upwellings, feeding them at intermediate Rayleigh numbers, or sometimes breaking before reaching them at higher Rayleigh numbers. These collisions result in a pulse-like behavior of the large-scale circulation generated by the large upwellings and downwellings. This corresponds to the short-timescale fluctuations. The long-timescale fluctuations may be due to a modification of the number and of the localization of the large convective cells. Such superposition of two scales of convection has already been noticed in turbulent isoviscous convection either numerically at infinite or finite Prandtl number [*Hansen and Ebel*, 1988; *Hansen et al.*, 1990; *Jarvis*, 1984; *Sirovich et al.*, 1989], or experimentally at Prandtl number of the order of unity [*Castaing et al.*, 1989; *Krishnamurti and Howard*, 1981]. At low Prandtl number the large-scale flow is held responsible for the exponent $\beta = 2/7$ in $Nu = Ra^{\beta}$ [*Castaing et al.*, 1989]. Convective flows without a lower thermal boundary layer, either in transient cooling experiments [*Davaille and Jaupart*, 1993] or in a fluid heated from within [*Grasset and Parmentier*, 1998; *Parmentier et al.*, 1994] show only small-scale destabilization. For all cases of this study, a lid is observed above the convective cells: The viscosity contrast

Table 2. Table of Results for a Newtonian Rheology for Both Time-Dependent and Steady State Calculations

b	c	Ra_0	Ra_{BL-N}	Nu	ν_{BL}	z_{BL}	T_i	$\dot{\varepsilon}_{max}$	v_{RMS}	σ_{Nu}
				Time-Dependent Calculations						
11.08	0.0	7	1.07×10^5	1.69	$10^{-4.19}$	0.51	0.870	320	30	0.00
11.08	0.0	21.5	4.50×10^5	2.20	$10^{-4.32}$	0.41	0.898	680	75	0.00
11.08	0.0	50	1.07×10^6	2.65	$10^{-4.33}$	0.40	0.900	1,130	130	0.00
11.08	0.0	115	2.52×10^6	3.19	$10^{-4.34}$	0.28	0.902	1,850	225	0.00
11.08	0.0	400	9.47×10^6	4.25	$10^{-4.37}$	0.21	0.909	4,300	590	0.01
11.08	0.0	1,350	3.02×10^7	6.40	$10^{-4.35}$	0.14	0.904	11,800	1,300	0.05
11.08	0.0	3,200	7.32×10^7	8.25	$10^{-4.36}$	0.11	0.906	20,800	2,250	0.11
11.08	0.0	4,900	1.10×10^8	9.52	$10^{-4.35}$	0.09	0.904	27,520	2,910	0.13
11.08	0.0	6,000	1.29×10^8	10.36	$10^{-4\ 33}$	0.09	0.900	31,850	3,250	0.10
11.08	0.0	7,500	1.59×10^8	11.10	$10^{-4.33}$	0.08	0.899	37,450	3,740	0.13
11.08	0.0	9,000	1.89×10^8	11.95	$10^{-4.32}$	0.08	0.898	42,500	4,125	0.14
11.08	0.0	11,000	2.30×10^8	12.65	$10^{-4.32}$	0.07	0.898	46,830	4,670	0.13
11.08	4.2	350	7.85×10^5	3.11	$10^{-3.35}$	0.36	0.793	590	76	0.00
11.08	4.2	500	1.53×10^6	3.38	$10^{-3.38}$	0.34	0.792	760	95	0.00
11.08	4.2	840	2.43×10^6	3.80	$10^{-3.46}$	0.30	0.799	1,130	130	0.00
11.08	4.2	1,680	4.46×10^6	4.31	$10^{-3.43}$	0.28	0.782	1,730	235	0.08
11.08	4.2	6,720	1.57×10^7	5.80	$10^{-3.37}$	0.21	0.749	3,940	550	0.08
11.08	4.2	16,800	4.09×10^7	7.73	$10^{-3.39}$	0.14	0.740	9,770	1,000	0.10
11.08	4.2	25,000	6.54×10^7	8.35	$10^{-3.42}$	0.13	0.744	15,400	1,100	0.06
13.0	0.0	37	4.70×10^6	3.20	$10^{-5.10}$	0.28	0.904	2,740	320	0.02
13.0	0.0	125	1.93×10^7	4.51	$10^{-5.19}$	0.20	0.919	7,680	800	0.02
13.0	0.0	295	4.55×10^7	5.68	$10^{-5.19}$	0.16	0.919	13,100	1,480	0.02
13.0	0.0	600	9.26×10^7	7.19	$10^{-5\ 19}$	0.13	0.919	22,670	2,370	0.05
13.0	0.0	1,100	1.61×10^8	9.18	$10^{-5.17}$	0.10	0.915	33,240	3,430	0.06
13.0	0.0	1,600	2.22×10^8	10.59	$10^{-5.14}$	0.09	0.911	41,800	3,960	0.11
13.0	0.0	2,100	2.99×10^8	11.75	$10^{-5.14}$	0.08	0.910	50,100	4,660	0.08
13.0	4.2	1,550	2.88×10^7	5.14	$10^{-4.27}$	0.16	0.807	7,700	580	0.04
13.0	4.2	2,480	4.11×10^7	6.28	$10^{-4.22}$	0.13	0.788	8,540	680	0.08
13.0	4.2	9,900	1.55×10^8	9.56	$10^{-4.19}$	0.08	0.769	23,900	1,520	0.15
13.0	4.2	19,000	2.71×10^8	11.59	$10^{-4.15}$	0.07	0.757	35,700	2,130	0.21
16.0	0.0	12	3.73×10^7	4.05	$10^{-6.49}$	0.23	0.934	9,500	1,010	0.03
16.0	0.0	20	6.73×10^7	4.55	$10^{-6.52}$	0.21	0.939	12,900	1,510	0.06
16.0	0.0	30	1.01×10^8	5.53	$10^{-6.49}$	0.17	0.934	19,700	1,960	0.04
16.0	0.0	43	1.28×10^8	6.42	$10^{-6.48}$	0.15	0.932	25,400	2,360	0.05
16.0	0.0	72	2.12×10^8	7.64	$10^{-6.47}$	0.12	0.931	35,900	3,460	0.03
16.0	0.0	140	3.75×10^8	9.83	$10^{-6.45}$	0.09	0.928	55,160	5,100	0.05
16.0	0.0	240	6.32×10^8	11.50	$10^{-6.42}$	0.08	0.924	71,300	6,630	0.12
16.0	4.2	300	8.84×10^7	6.35	$10^{-5.47}$	0.13	0.821	12,704	980	0.04
16.0	4.2	600	1.67×10^8	7.74	$10^{-5.44}$	0.10	0.811	20,990	1,490	0.03
				Steady State Calculations						
11.08	0.0	7	1.11×10^5	1.69	$10^{-4.19}$	0.52	0.871	330	30	...
11.08	0.0	115	2.51×10^6	3.19	$10^{-4.33}$	0.28	0.900	1,870	220	...
11.08	0.0	400	9.86×10^6	4.35	$10^{-4.38}$	0.21	0.911	3,970	580	...
11.08	0.0	1,350	3.72×10^7	5.79	$10^{-4.43}$	0.16	0.921	8,360	1,400	...
11.08	0.0	3,200	9.31×10^7	7.06	$10^{-4.46}$	0.13	0.926	14,860	2,570	...
11.08	0.0	4,900	1.49×10^8	7.77	$10^{-4.48}$	0.12	0.930	20,770	3,450	...
11.08	4.2	350	7.93×10^5	3.12	$10^{-3.35}$	0.25	0.792	590	80	...
11.08	4.2	840	2.42×10^6	3.85	$10^{-3.45}$	0.21	0.796	1,080	130	...
11.08	4.2	6,720	3.21×10^7	6.31	$10^{-3.67}$	0.13	0.812	4,650	550	...
11.08	4.2	25,000	1.65×10^8	8.59	$10^{-3.81}$	0.10	0.829	15,040	1,430	...
13.0	0.0	125	2.09×10^7	4.35	$10^{-5.22}$	0.21	0.925	5,630	820	...
13.0	0.0	600	1.14×10^8	6.27	$10^{-5.28}$	0.15	0.935	14,080	2,580	...
13.0	0.0	1,600	3.29×10^8	7.82	$10^{-5.31}$	0.12	0.941	32,490	5,150	...
13.0	0.0	2,100	4.37×10^8	8.30	$10^{-5.32}$	0.11	0.942	39,500	6,210	...
16.0	0.0	240	1.01×10^9	7.95	$10^{-6.62}$	0.12	0.953	60,080	1,430	...

Table 3. Table of Results for a Non-Newtonian Rheology and Either Time-Dependent or Steady State Calculations

$b/3$	$c/3$	Ra_0	$Ra_{\text{BL-nN}}$	$Ra_{\text{BL-eff}}$	Nu	$\nu_{\text{eff-BL}}$	z_{BL}	T_i	$\dot{\varepsilon}_{\max}$	v_{RMS}	σ_{Nu}
				Time-Dependent Calculations							
11.08	4.2	5	78.4	0.00	1.00	$10^{-1.37}$	0.40	0.400	0	0	0.00
11.08	4.2	10	1.57×10^4	8.71×10^5	2.43	$10^{-4.94}$	0.32	0.787	1,370	110	0.02
11.08	4.2	15	3.36×10^4	4.13×10^6	3.06	$10^{-5.44}$	0.27	0.795	2,930	190	0.03
11.08	4.2	25	5.54×10^4	1.2×10^7	3.64	$10^{-5.68}$	0.22	0.776	6,470	300	0.04
11.08	4.2	35	7.84×10^4	2.21×10^7	4.52	$10^{-5.80}$	0.19	0.760	8,040	370	0.16
11.08	4.2	56	1.14×10^5	4.06×10^7	5.03	$10^{-5.86}$	0.16	0.744	12,970	570	0.04
11.08	4.2	65	1.39×10^5	5.23×10^7	5.32	$10^{-5.91}$	0.14	0.745	14,150	680	0.05
11.08	4.2	100	2.14×10^5	1.12×10^8	6.51	$10^{-6.05}$	0.11	0.735	24,400	970	0.06
9.0	0.0	5	2.30×10^4	1.99×10^6	2.00	$10^{-5.60}$	0.47	0.938	1,830	170	0.02
9.0	0.0	10	4.64×10^4	5.37×10^5	2.66	$10^{-5.73}$	0.48	0.938	1,350	420	0.01
9.0	4.2	30	4.41×10^3	8.26×10^4	2.05	$10^{-3.44}$	0.48	0.718	430	50	0.00
9.0	4.2	40	9.39×10^3	4.49×10^5	2.54	$10^{-4.05}$	0.29	0.743	890	80	0.00
9.0	4.2	65	1.43×10^4	1.27×10^6	2.98	$10^{-4.29}$	0.25	0.711	1,580	120	0.00
9.0	4.2	95	2.20×10^4	2.68×10^6	3.61	$10^{-4.45}$	0.22	0.711	3,070	180	0.09
9.0	4.2	148	3.89×10^4	5.76×10^6	4.49	$10^{-4.60}$	0.19	0.691	4,800	270	0.10
9.0	4.2	176	4.44×10^4	7.68×10^6	4.78	$10^{-4.64}$	0.18	0.681	5,740	310	0.08
9.0	4.2	230	5.88×10^4	1.45×10^7	5.33	$10^{-4.80}$	0.13	0.675	7,830	390	0.12
7.3	0.0	130	1.09×10^5	3.12×10^7	6.19	$10^{-5.38}$	0.19	0.922	17,500	1,740	0.08
7.3	4.2	95	4.8×10^3	1.22×10^5	2.56	$10^{-3.11}$	0.42	0.693	430	50	0.00
7.3	4.2	176	9.12×10^3	5.83×10^5	3.23	$10^{-3.52}$	0.19	0.658	1,190	90	0.00
7.3	4.2	256	1.24×10^4	1.14×10^6	3.61	$10^{-3.65}$	0.19	0.634	1,540	120	0.10
7.3	4.2	400	1.79×10^4	2.15×10^6	4.40	$10^{-3.73}$	0.15	0.599	2,890	180	0.16
7.3	4.2	475	2.26×10^4	3.36×10^6	4.82	$10^{-3.85}$	0.12	0.601	3,451	210	0.17
7.3	4.2	620	3.21×10^4	5.53×10^6	5.40	$10^{-3.95}$	0.11	0.605	5,140	270	0.20
				Steady State Calculations							
11.08	4.2	3	2.90×10^2	0.00	1.00	$10^{-0.93}$	0.55	0.546	0	0	...
11.08	4.2	10	2.12×10^4	1.05×10^6	2.23	$10^{-5.02}$	0.37	0.833	1,080	100	...
11.08	4.2	15	3.78×10^4	2.38×10^6	2.50	$10^{-5.20}$	0.33	0.833	1,610	160	...
11.08	4.2	25	6.97×10^4	5.60×10^6	2.87	$10^{-5.35}$	0.29	0.825	2,570	240	...
9.0	4.2	30	4.47×10^3	8.26×10^4	2.05	$10^{-3.44}$	0.35	0.720	430	50	...
9.0	4.2	65	2.53×10^4	1.39×10^6	2.90	$10^{-4.33}$	0.27	0.790	1,490	140	...
9.0	4.2	148	6.33×10^4	5.01×10^6	3.49	$10^{-4.53}$	0.22	0.777	2,840	260	...
7.3	4.2	55	2.99×10^2	0.00	1.00	$10^{-0.35}$	0.55	0.546	0	0	...
7.3	4.2	95	4.80×10^3	1.22×10^5	2.56	$10^{-3.11}$	0.27	0.693	430	50	...
7.3	4.2	176	1.28×10^4	5.96×10^5	3.09	$10^{-3.53}$	0.23	0.721	1,040	100	...
7.3	4.2	256	2.05×10^4	1.23×10^6	3.40	$10^{-3.68}$	0.21	0.723	1,500	140	...
7.3	4.2	400	3.48×10^4	2.64×10^6	3.80	$10^{-3.82}$	0.19	0.721	2,200	200	...

is so high that the upper part of the box is not convecting.

4. Results for a Newtonian Rheology

Calculations are carried out for different values of the parameter b which characterizes the temperature dependence of the viscosity ($b = 11.08$, $b = 13.0$, or $b = 16.0$, corresponding to a total viscosity contrast ranging from 6.5×10^4 to 8.9×10^6) and for two different values of the parameter c which characterizes the depth dependence of the viscosity ($c = 0.0$ or $c = 4.2$, corresponding to a total viscosity contrast ranging from 1 to 66.7). Some calculations have been done with $c = 7.0$, but in those cases, the total viscosity drop across the UTBL is so small that there is no longer a rigid lid, and the viscosity is very high in the lower part of the box. Therefore these simulations have been withdrawn.

4.1. Identification of Two Different Regimes

In Figure 5 the Nusselt number Nu is plotted versus $b^{-4/3}Ra_{\text{BL}-N}^{1/3}$ (relationship obtained with the boundary layer stability analysis [*Davaille and Jaupart*, 1993; *Doin et al.*, 1997; *Solomatov*, 1995]). We note that for chaotic simulations at high Nusselt numbers, the

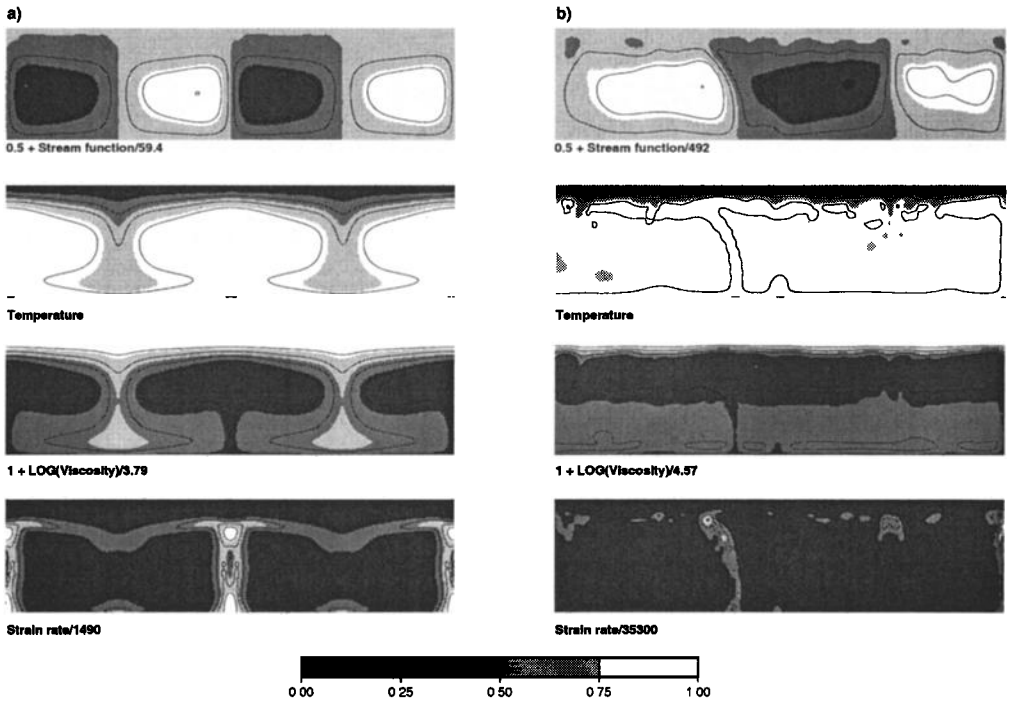

Figure 2. Stream function, temperature, viscosity, and strain rate fields for a Newtonian rheology (a) with $Ra_0 = 350$, $b = 11.08$, and $c = 4.2$, and (b) with $Ra_0 = 2480$, $b = 13.0$, and $c = 4.2$. Variables are dimensionless and divided to be bracketed by 0.0 and 1.0.

fit between the numerical results and the prediction of the boundary layer analysis is good (Nusselt root-mean-square misfit of 0.40). However, this law does not apply for the low Nusselt number cases corresponding to a steady state flow (Nusselt root-mean-square misfit of 0.70). In order to check whether this difference of behavior between the points at high and low Nusselt number was due to the transition between steady state and time-dependent regimes, we performed some calculations at high Nusselt number in a forced steady state (using the overrelaxation option of the numerical code). The results from the steady state runs and the results

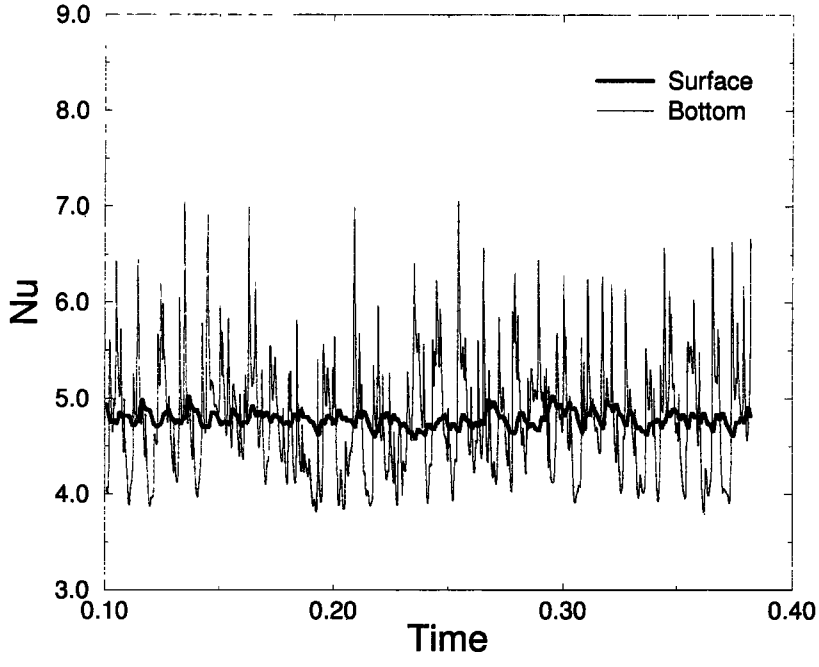

Figure 3. Example of surface (thick line) and bottom (thin line) Nusselt numbers versus dimensionless time in the turbulent regime for a non-Newtonian rheology, with $Ra_0 = 176$, $b = 9.0$, and $c = 4.2$.

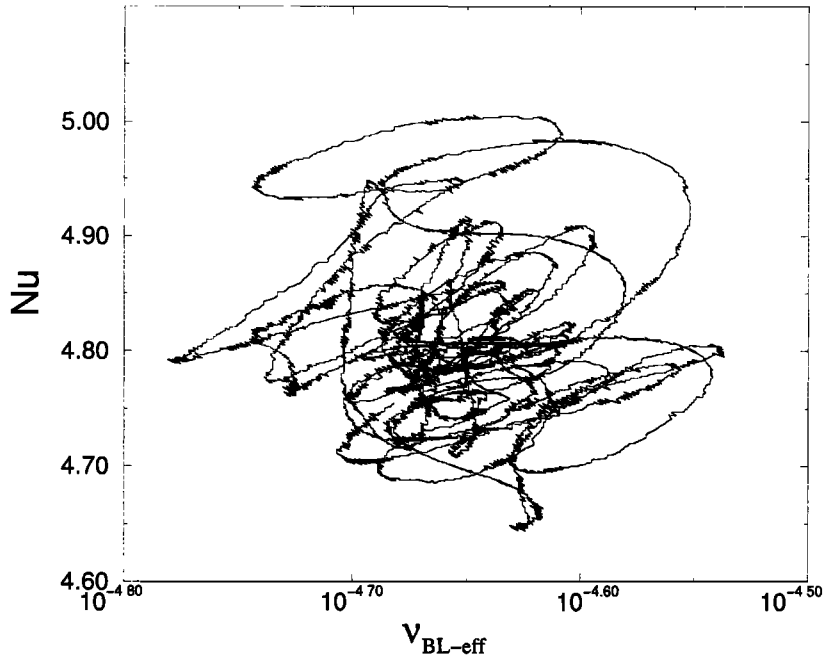

Figure 4. Average over short-term fluctuations of surface Nusselt number versus effective viscosity at the base of the upper thermal boundary layer (UTBL) drawn as function of time. It indicates a chaotic behavior (case with a non-Newtonian rheology, $Ra_0 = 176$, $b = 9.0$, and $c = 4.2$).

of time-dependent calculations at low Nusselt number (showing no destabilization) follow the same trend. For these steady state runs, we obtain $Nu \propto Ra_{BL-N}^{1/5}$, as predicted by *Fowler* [1985] and *Morris and Canright* [1984].

4.2. Turbulent Regime

We now analyze the Nusselt-Rayleigh number relationship for the runs characterized by a time-dependent regime at high Nusselt number. In the experiments of *Davaille and Jaupart* [1993], the exponent of b was found equal to (-4/3), but only one thermal boundary layer was present, the bottom of the box being adiabatic. Therefore only the destabilization process at the base of the UTBL was operating. In the simulations described here, the instabilities interact with the large-scale flow bounding the two boundary layers. The large-scale flow creates a shear stress at the bottom of the upper thermal boundary layer and could modify locally the critical Rayleigh number for the onset of instability and change the heat transfer law. To see wether the exponent (-4/3) in b applies here, we compute the values of $\beta(b) \pm \sigma_{\beta(b)}$ with a linear regression in the form $Nu = \beta(b) Ra_{BL-N}^{1/3}$ separately for each value of b = 11.08, 13.0, 16.0, and for c = 0.0. The function $0.52b^{4/3}$ fits well, within the error bars, $\beta(b)$. Therefore the interaction between the two scales of convection, the large-scale and the secondary flows, does not significantly change the exponent of b in the scaling relation for the heat transport. We note that the $Nu = 0.52b^{-4/3} Ra_{BL-N}^{1/3}$ relationship is also the same as that obtained by *Doin et al.* [1997].

The pressure dependence of the viscosity should be taken into account in the law characterizing the heat transport in the turbulent regime. The effective viscous temperature scale is the temperature drop required for an increase of viscosity by e at the base of the upper thermal boundary layer. It must be increased for a given temperature gradient to offset the increase of viscosity with depth: The inverse of this effective viscous temperature scale is b_{eff}. Assuming a constant temperature gradient given by the Nusselt number within the UTBL, we get

$$b_{\text{eff}} = b - \frac{c}{Nu} \tag{7}$$

However, the temperature profile may not be linear at the base of the lithosphere (see Figure 6). *Sleep* [1994] suggested that the thermal gradient in the active boundary layer is about half the conductive gradient in the lid. Therefore the corrective term in pressure, α, is not necessarily equal to 1. We search for a value of b_{eff} of the form

$$b_{\text{eff}} = b - \alpha \frac{c}{Nu} \tag{8}$$

A linear regression is done with the points in the chaotic regime and the points of *Doin et al.* [1997]. It yields $\alpha = 1.0 \pm 0.1$ (see Figure 7). Thus α is not significantly different from 1.0: The temperature gradient across the UTBL is almost linear. However, this will not be true in the non-Newtonian case.

Once this correction is taken into account (see Figure 8), we obtain a good agreement of the results in the turbulent regime with the following law (Nusselt root-mean-square misfit of 0.35):

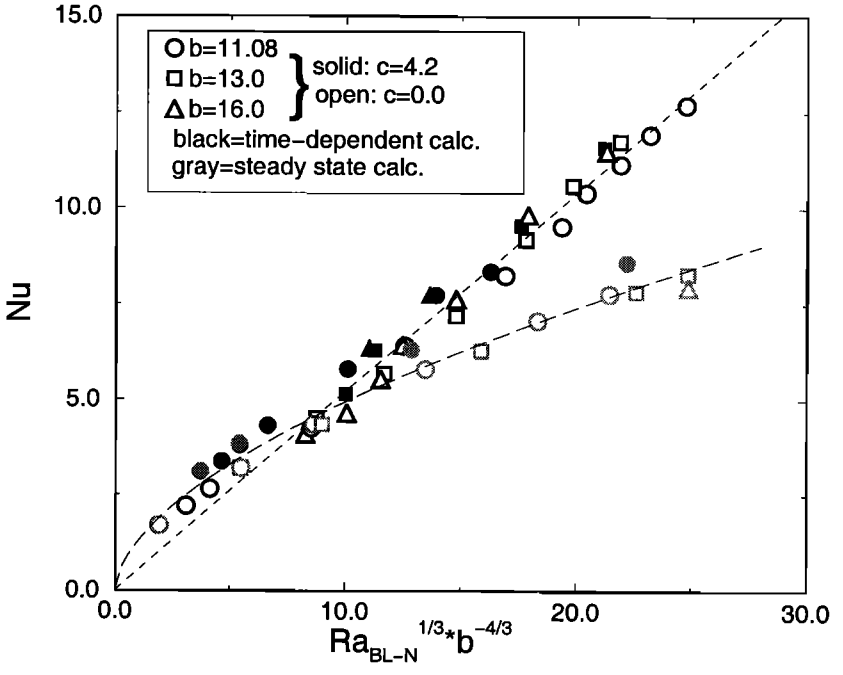

Figure 5. The surface Nusselt number is plotted as a function of $Ra_{BL-N}^{1/3} b^{-4/3}$. A linear regression of the form $y = a_1 x$ for the turbulent regime yields $a_1 = 0.52$ (short-dashed line). Nonlinear curve fitting of the form $y = a_2 x^{a_3}$ for the stationary regime yields $a_2 = 1.28$ and $a_3 = 0.59$ (long-dashed line). Black symbols are used for time-dependent calculations and gray for steady state calculations. Open symbols represent calculations with no pressure dependence of the viscosity ($c = 0.0$), and solid symbols represent calculations with a pressure dependence $c = 4.2$. Circles are plotted for calculations with a temperature dependence of the viscosity $b = 11.08$, squares for $b = 13.0$, and triangles for $b = 16.0$.

$$Nu = 0.52 Ra_{BL-N}^{1/3} \left(b - 1.0\frac{c}{Nu}\right)^{-4/3} \quad (9)$$

The previous analysis does not work if the Rayleigh number is calculated with the viscosity at the bottom or at the middle of the box (Nusselt root-mean-square misfit of 1.7 with α taken as a free parameter). This, together with the exponent 1/3 for the Rayleigh number, seems to indicate that destabilization at the base of the upper thermal boundary layer does control the heat transfer.

The heat transfer through a "continental lithosphere" moving above a convecting mantle (data of *Doin et al.* [1997]) fits this law very well, even at low Nusselt number (see Figure 9). This indicates that the thickness of the continental lithosphere is controlled by the development of instabilities at its base. Therefore whatever the thermal state of the Earth (i.e., whatever Ra), relation (9) will well describe the heat transfer through the lithosphere at equilibrium.

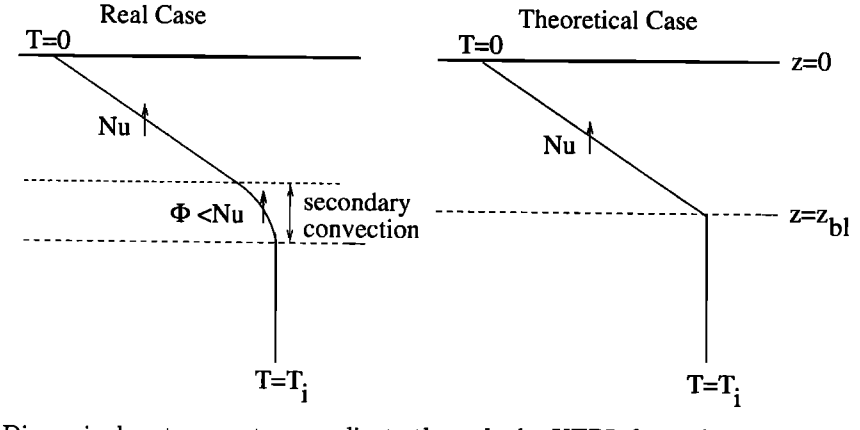

Figure 6. Dimensionless temperature gradients through the UTBL for a theoretical and a real case. The temperature gradient $\Phi = Nu/\alpha$ in the destabilized layer can be different from the surface Nusselt number Nu. This effect should be taken into account when $(d\ln\nu/dT)_{BL}$ across the destabilized layer is calculated.

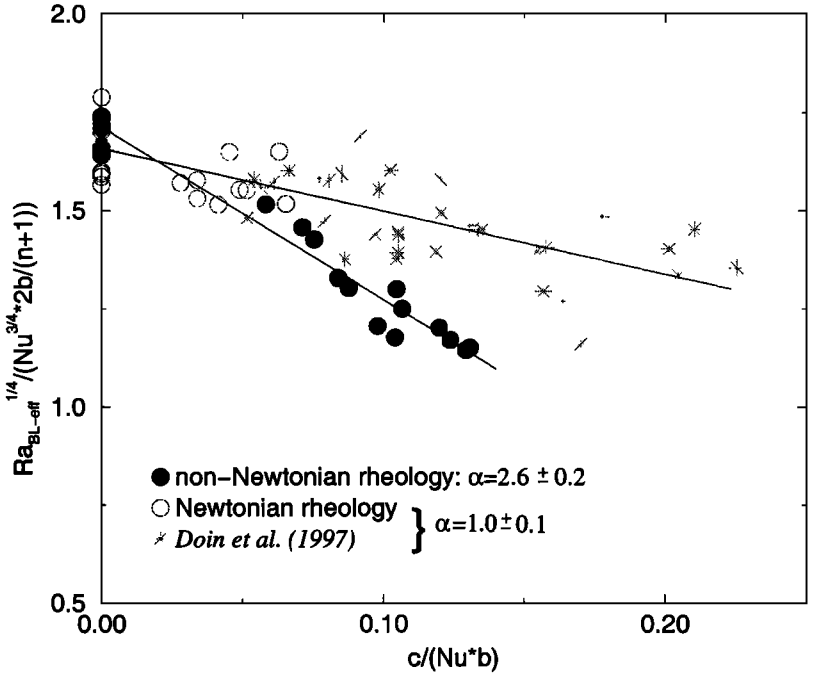

Figure 7. Linear regressions performed to compute α in $Nu = \beta_1 Ra_{\text{BL-eff}}^{1/3}\{[2/(n+1)](b-\alpha c/Nu)\}^{-4/3}$ for turbulent flows. The rheology is Newtonian for open circles (this study) or asterisks [*Doin et al.*, 1997], and non-Newtonian for solid circles.

4.3. Stationary Regime

The same correction in pressure of the "viscous" temperature scale is applied. The steady state data resulting either from time-dependent calculations or from steady state calculations fit the scaling relation (10) (see Figure 10) (Nusselt root-mean-square misfit of 0.16 for time-dependent calculations) :

$$Nu = 2.0 Ra_{\text{BL}-N}^{1/5}\left(b - 1.0\frac{c}{Nu}\right)^{-1} \qquad (10)$$

This relationship agrees well with the data of *Moresi and Solomatov* [1995] and the prediction of the asymptotic boundary layer theory by *Fowler* [1985]. It differs from that of *Morris and Canright* [1984], who predicted a different exponent for b ($Nu \propto Ra^{1/5}b^{-6/5}$). *Fowler*

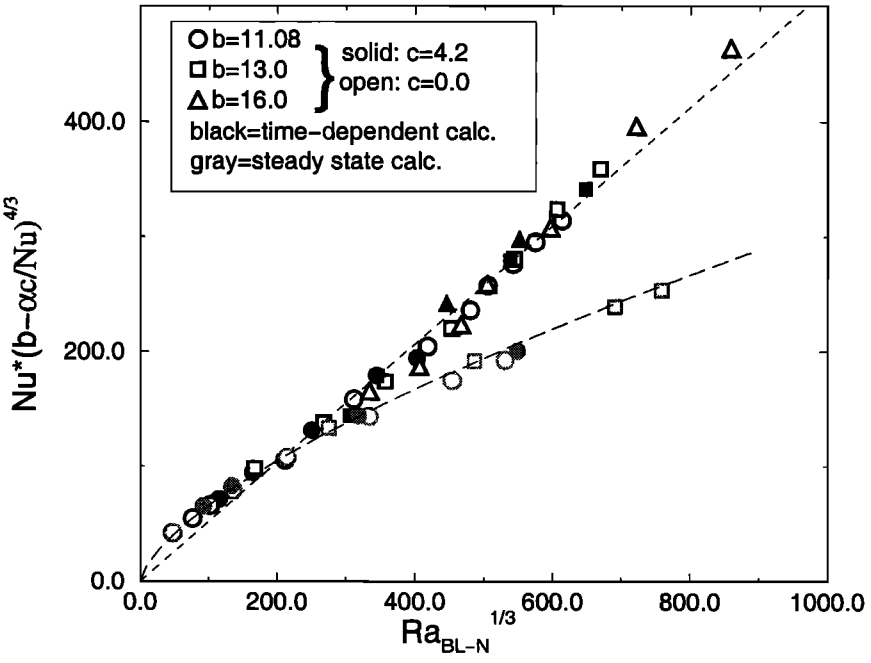

Figure 8. $Nu(b-1.0c/Nu)^{4/3}$ plotted versus $Ra_{\text{BL}-N}^{1/3}$. A linear regression of the form $y = a_1 x$ for the turbulent regime yields $a_1 = 0.52$ (short-dashed line). Nonlinear curve fitting of the form $y = a_2 x^{a_3}$ for the stationary regime yields $a_2 = 2.91$ and $a_3 = 0.68$ (long-dashed line). For the remaining symbols, see Figure 5.

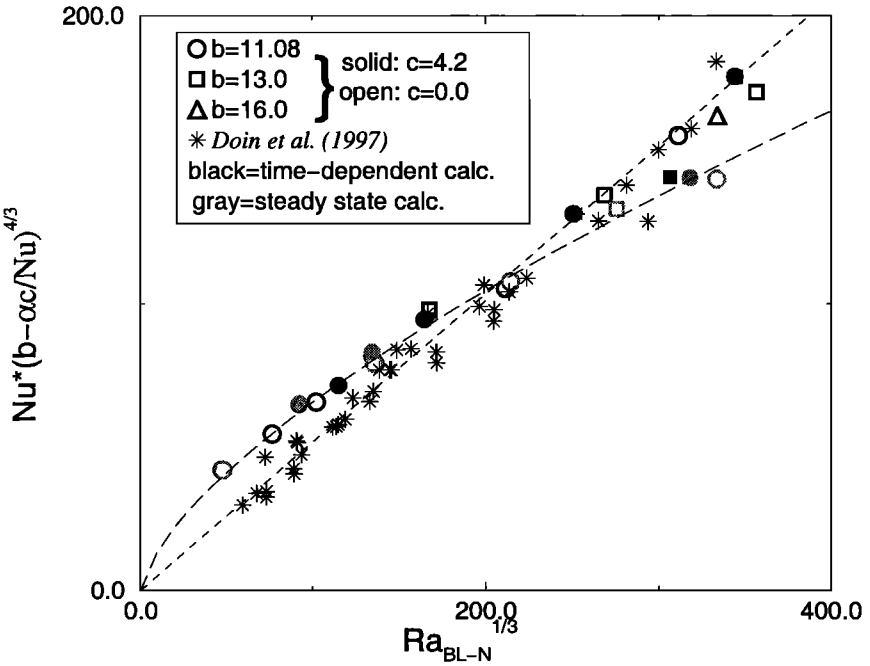

Figure 9. Detail of Figure 8. Added points (asterisks) from *Doin et al.* [1997] correspond to the heat transfer through a continental lithosphere moving above a convecting mantle ($b = 11.08$ to 17.1, $c = 0.0$ to 6).

[1985] and *Moresi and Solomatov* [1995] did not include the pressure dependence of the viscosity. They used a Rayleigh number calculated with the bottom viscosity. We notice here that when values of c are different from 0, the fit is not good with a Rayleigh number calculated with the bottom viscosity or with the middepth viscosity. This is somewhat surprising but confirms mean field results obtained by *Fleitout and Yuen* [1984b]: Heat transfer for pressure-dependent stationary convection is also controlled by ν_{BL}.

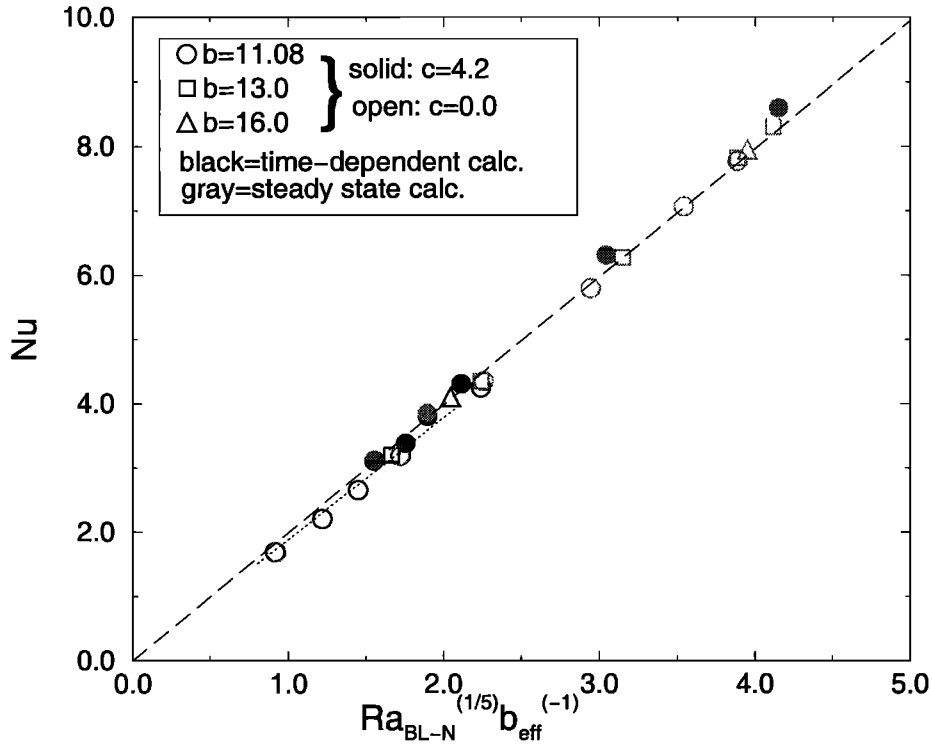

Figure 10. Nusselt number plotted versus $Ra_{BL-N}^{1/5} b_{eff}^{-1}$, for stationary flows resulting from either time-dependent or steady state calculations. Long dashed line is *Fowler* [1985]'s prediction and dotted line represents *Moresi and Solomatov*'s [1995] results (symbols as in Figure 5).

4.4. Domains of the Two Regimes

Based on linear stability analysis, *Stengel et al.* [1982] suggested that a rigid lid develops at the surface when the total viscosity contrast $\Delta\nu$ is larger than exp(8). We checked that our simulations present a rigid conductive lid (the velocity at lid half-depth ($z_{BL}/2$) is < 0.005 times the interior velocity). Therefore our heat transfer parameterization should be the same as that obtained with stress-free experiments in the rigid lid regime. However, in the latter experiments, the conditions necessary to obtain a stagnant lid at the surface are still not well constrained [*Giannandrea and Christensen*, 1993; *Grasset and Parmentier*, 1998; *Ogawa et al.*, 1991]. This may explain why *Deschamps* [1997], using steady state numerical calculations, with free boundary conditions, obtained in the stagnant lid regime a parameterization very different from equation (9) and from that of *Moresi and Solomatov* [1995].

Using our data, we are now able to divide the stagnant lid regime into a steady state regime and a turbulent regime (see Figure 11). Of course, the limit between these two new domains would be better defined with more results. If we assume that at the transition, the "stationary" Nusselt number equals the "turbulent" Nusselt number (equations (9) and (11)), then the value of Ra_{BL-N} at the transition is given by $Ra_{BL-N} = 2.4 \times 10^4 [b - c/Nu]^{5/2}$ (dotted-dashed curve in Figure 11). It corresponds to a viscosity at the base of the lithosphere of 9.3×10^{18} Pa s for a height of 670 km and other parameters defined in Table 2. If we suppose that the viscosity in the asthenosphere is 1 order of magnitude smaller than the mean upper mantle viscosity (which appears to be of the order of 3×10^{20} Pa s [e.g., *Lambeck et al.*, 1998; *Ricard and Vigny*, 1989]), then the Earth is in the turbulent regime. Note that Moresi and Solomatov's results are mostly in the stationary domain (see Figure 11).

5. Interpretation for a Non-Newtonian Rheology

As in the case of a Newtonian rheology, time-dependent calculations are performed for different values of the temperature dependence of the viscosity ($b = 21.9$, $b = 27.0$, or $b = 33.24$) and for two different values of the depth dependence of the viscosity ($c = 0.0$ or $c = 12.6$). In some time-dependent calculations, Ra_0 (the surface Rayleigh number) has been continuously increased during the run. This increase as a function of time is slow enough to allow the convection to be in a quasi-static equilibrium (short-term average of bottom and surface heat flow are equal). For those special runs, variables are smoothed like in Figure 4 (see section 3).

5.1. Comparison With the Newtonian Rheology

Almost all the results obtained in the case of a non-Newtonian rheology with time-dependent calculations depend strongly on time. Therefore results are plotted using the turbulent regime's law found for the Newto-

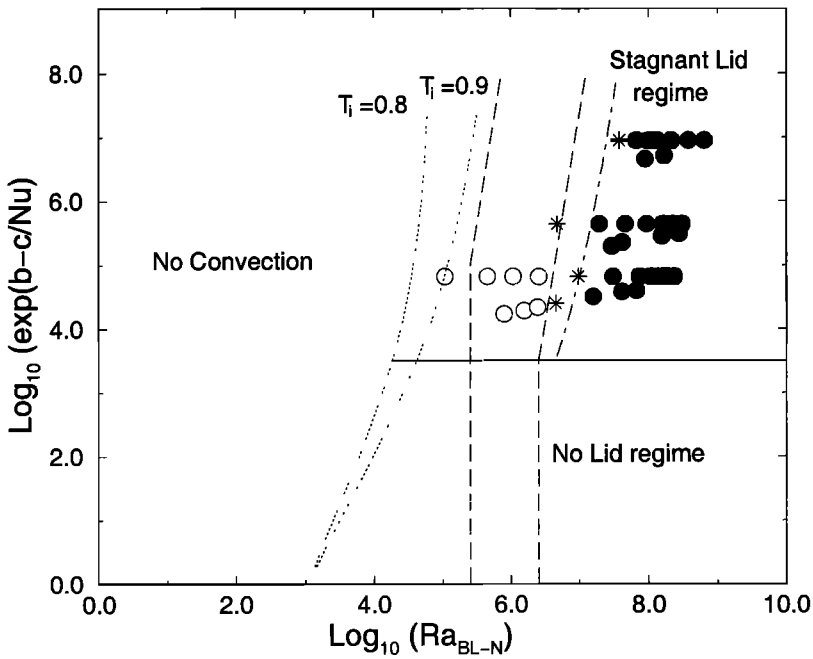

Figure 11. Regimes of convection identified in a two-dimensional (2-D) plot (effective viscosity contrast versus Ra_{BL-N}). The results of time-dependent calculations in Newtonian rheology are represented in the steady state regime by open circles, at the transition by asterisks, and in the turbulent regime by solid circles. Dotted lines give the critical Rayleigh number based on the viscosity at $T_i = 0.8$ and at $T_i = 0.9$. Black line from *Stengel et al.* [1982] separates the stagnant lid regime from the no-lid regime. Dashed area is the domain of *Moresi and Solomatov*'s [1995] study. Dash-dotted line is the transition found between the stationary and the turbulent regime (see text).

nian rheology:

$$Nub_{\text{eff}}^{4/3} \propto Ra_{\text{BL-eff}}^{1/3} \tag{11}$$

The use of $Ra_{\text{BL-eff}}$ enables one to compare non-Newtonian and Newtonian simulations.

The same correction in pressure is done for b_{eff}: $b_{\text{eff}} = b - \alpha c/Nu$. By a linear regression, α is found to be equal to 2.6 ± 0.2 (see Figure 7). Thus α in the non-Newtonian case is larger than in the Newtonian case. This seems to indicate that the curvature of the temperature gradient is larger in the case of a non-Newtonian rheology. However, for small Nusselt numbers ($Nu < 2$), this corrective term is too high and the relation between Nu and $Ra_{\text{BL-eff}}$ (equation (11)) does not apply.

Christensen [1983] showed that the properties of non-Newtonian flow can be closely imitated by a Newtonian fluid with a reduced value of the activation energy γE_a^* and $\gamma = 0.3 - 0.5$. The analysis of our results for a non-Newtonian rheology fits the following law (Nusselt root-mean-square misfit of 0.34) (see Figure 12):

$$Nu = 0.48 Ra_{\text{BL-eff}}^{1/3} \left(\frac{1}{2}(b - 2.6\frac{c}{Nu})\right)^{-4/3} \tag{12}$$

Therefore non-Newtonian results superimpose on Newtonian results if the activation energy is divided by 2 ($\gamma = 0.5$).

5.2. Non-Newtonian Parameterization Proposed by Solomatov

Solomatov [1995] extended the boundary layer stability analysis to the non-Newtonian rheology and obtained

$$Nu \propto \left(\frac{Ra_{\text{BL-nN}}}{Ra_{\text{cr}}}\right)^{\frac{n}{n+2}} \tag{13}$$

where

$$Ra_{\text{cr}} = Ra_{\text{cr-is}} \left(\frac{e}{4(n+1)}\right)^{\frac{2(n+1)}{n}} (b - \alpha\frac{c}{Nu})^{\frac{2(n+1)}{n}} \tag{14}$$

$Ra_{\text{cr-is}}$ is the critical Rayleigh number for an isoviscous case and is tentatively estimated as $Ra_{\text{cr-is}} = 1568^{1/n} 20^{(n-1)/n}$. Note that in the expression of Ra_{cr}, we replace b by $b_{\text{eff}} = b - \alpha c/Nu$. A fit through our data yields, for $n = 3$

$$Nu = 0.89 Ra_{\text{BL-nN}}^{3/5} (b - \alpha\frac{c}{Nu})^{-8/5} \tag{15}$$

$$\text{or } Nu = 0.75 \left(\frac{Ra_{\text{BL-nN}}}{Ra_{\text{cr}}}\right)^{3/5} \tag{16}$$

Figure 13 shows us that a few points resulting from time-dependent calculations do not follow this law. The Nusselt root-mean-square misfit using (15) without these points is 0.22. These simulations either do not show

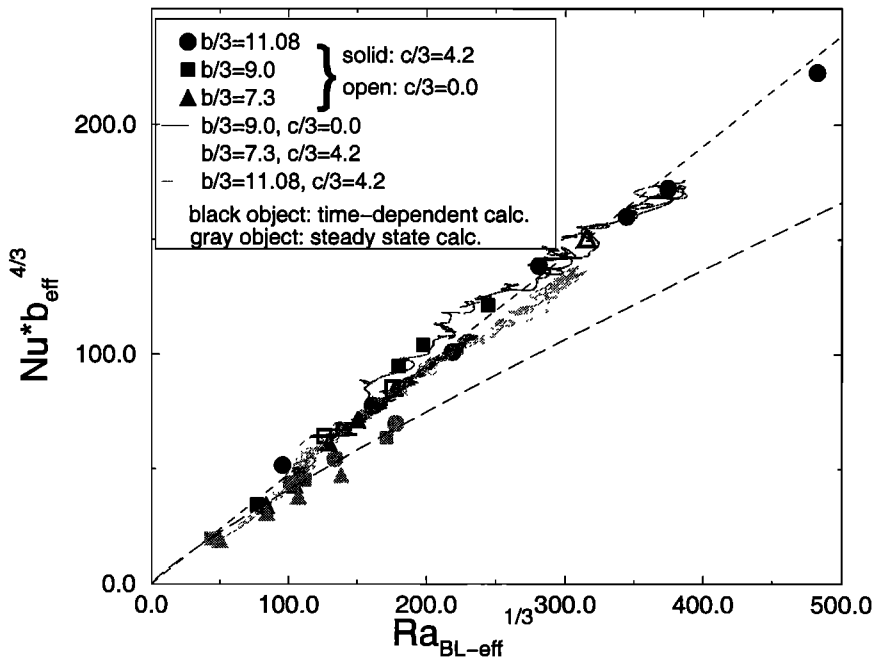

Figure 12. $Nu \times \frac{1}{2}(b - 2.6c/Nu)^{4/3}$ plotted versus $Ra_{\text{BL-eff}}^{1/3}$ for a non-Newtonian rheology, with time-dependent and steady state calculations. A linear regression of the form $y = a_1 x$ for the turbulent regime yields $a_1 = 0.48$ (short-dashed line). Nonlinear curve fitting of the form $y = a_2 x^{a_3}$ for the stationary regime yields $a_2 = 0.75$ and $a_3 = 0.87$ (long-dashed line). Black symbols are pictured for time-dependent calculations and gray symbols for steady state calculations. Open symbols represent simulations done with no pressure dependence of the viscosity. Solid symbols show simulations done with $c/3 = 4.2$. Circles represent results calculated with a temperature dependence of the viscosity of $b/3 = 11.08$, squares are calculated with $b/3 = 9.0$, and triangles are calculated with $b/3 = 7.3$. Solid, heavily shaded, and lightly shaded lines represent simulations for which Ra_0 has been increased slowly, with a temperature dependence of the viscosity of $b/3 = 11.08$, $b/3 = 9.0$, and $b/3 = 7.3$, respectively.

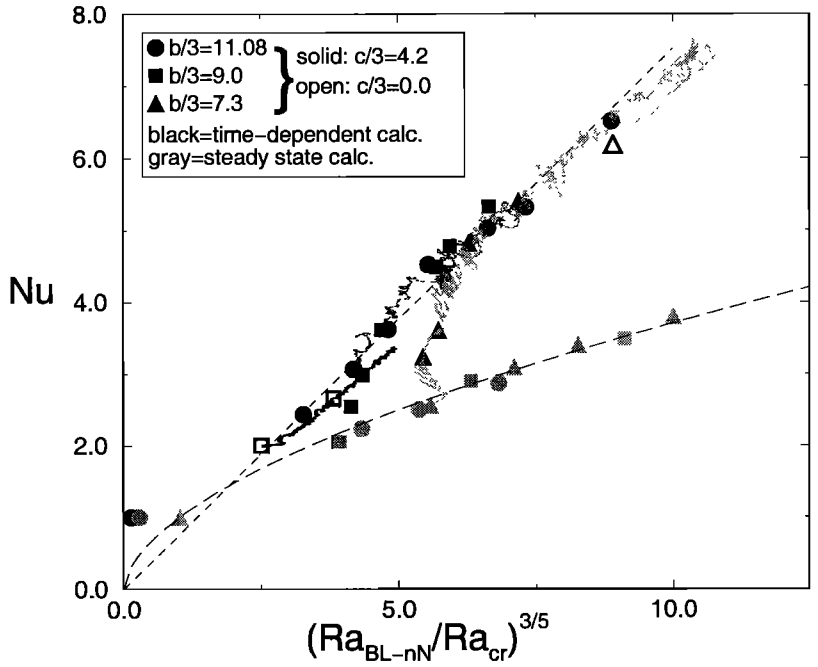

Figure 13. Nusselt number plotted according to the boundary layer stability analysis extended by *Solomatov* [1995]: $(Ra_{\text{BL-nN}}/Ra_{\text{cr}})^{3/5}$ (Ra_{cr} is defined in the text). A linear regression of the form $y = a_1 x$ for the turbulent regime yields $a_1 = 0.75$ (short-dashed line). Nonlinear curve fitting of the form $y = a_2 x^{a_3}$ for the stationary regime yields $a_2 = 1.00$ and $a_3 = 0.57$ (long-dashed line). Other symbols and curves are defined in Figure 12.

destabilization at the base of the lithosphere and do not depend on time (stable cases), or do not vary much with time (their temperature, viscosity, and stream function fields are only slightly time-dependent). Therefore results of steady state calculations are also plotted on Figure 13. In this graph, one can easily define two trends. At low Nusselt number, the results of time-dependent calculations join the steady state curve. It is also easy to identify results in the transition between the turbulent regime and the stationary regime. Both trends also exist in Figure 12; however, they are not so clearly distinct. Therefore the same two regimes as in Newtonian rheology exist in non-Newtonian rheology, a turbulent regime characterized by a strong dependence with time and destabilization of the thermal boundary layers and, at small Nusselt numbers, a stationary regime characterized by no dependence with time and only one scale of convection, the large-scale flow. *Reese and Solomatov* [1998] extended the asymptotic boundary layer theory to non-Newtonian stationary flows with a stagnant lid. They proposed two fitting formulas, $Nu \propto Ra_{\text{BL-nN}}^{1/3} b^{-1}$ (large lid slope) or $Nu \propto Ra_{\text{BL-nN}}^{1/3} b^{-4/3}$ (flat roof); however, our steady state results do not follow any of them. We found no explanation for this discrepancy.

5.3. Domains of the Two Regimes

Solomatov [1995] extended the analysis of *Stengel et al.* [1982] to a non-Newtonian rheology with stress exponent n. He found a stagnant lid regime for $b > 4(n + 1)$. This transition between the stagnant lid regime and the whole layer convection regime has been drawn in Figure 14. Some numerical experiments with a strongly temperature-dependent viscosity have been done by *Solomatov and Moresi* [1997] to identify the small viscosity contrast regime, the transitional regime, and the stagnant lid regime as in the Newtonian case. Here, we only study the stagnant lid regime. In Figure 14 the transition between the stationary domain (only one scale of convection) and the turbulent regime (two scales of convection) is broad (as denoted by transition points shown by asterisks). The limit between these two domains is uncertain given the scarcity of our points in steady state. It may depend on both the Rayleigh number and b. As the law for steady state calculations is not known, the transition cannot also be derived theoretically.

6. Discussion

Two-dimensional convection has been studied with either Newtonian or non-Newtonian temperature- and pressure-dependent rheology, and with either time-dependent calculations or steady state calculations. The main findings of this study are as follows:

1. Our data concerning the relationship between Nusselt and Rayleigh number in the chaotic regime yield $Nu = 0.52 Ra_{\text{BL-eff}}^{1/3} b_{\text{eff}}^{-4/3}$. This is very close to the law proposed by *Davaille and Jaupart* [1993] with transient cooling experiments and by *Doin et al.* [1997] with a

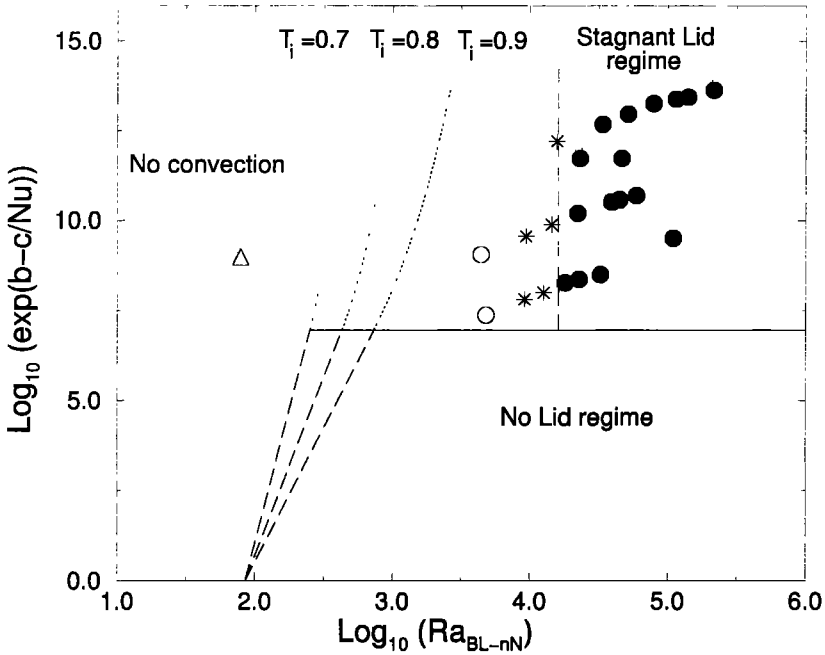

Figure 14. Regimes of convection identified on a 2-D plot (effective viscosity contrast versus $Ra_{\text{BL-nN}}$). Points presented here are results of time-dependent calculations in the case of a non-Newtonian rheology. Symbols are defined in Figure 11. Dotted lines give the critical Rayleigh number based on the viscosity at $T_i = 0.7$, $T_i = 0.8$, and $T_i = 0.9$ (dashed lines are extrapolated from dotted lines). The solid line separates the stagnant lid regime from the no-lid regime [*Solomatov*, 1995].

continental lithosphere moving above a convecting mantle.

2. We introduce a corrective term in pressure for the calculation of $(-\partial \ln\nu/\partial T)^{-1}_{\text{BL}} = b_{\text{eff}} = b - \alpha c/Nu$ where $\alpha = 1.0 \pm 0.1$ for the Newtonian rheology and $\alpha = 2.6 \pm 0.2$ for the non-Newtonian rheology.

3. The same heat flow is obtained in non-Newtonian and Newtonian rheologies if the activation energy is divided by 2 and the activation volume is divided by 0.8.

4. In both rheologies, the stationary and the turbulent regimes are shown to be characterized by different $Nu = f(Ra)$ parameterizations corresponding to the asymptotic boundary layer theory and the boundary layer stability analysis, respectively. The transition between both regimes has been identified.

Of course, parameterizations obtained with three-dimensional (3-D) simulations would be more appropriate to the Earth. However, the Nu versus Ra relationship in a 3-D, rigid lid regime, and strongly temperature-dependent viscosity, has until now been restricted to steady state cases [*Ratcliff et al.*, 1995, 1996, 1997], whereas we show that the turbulent regime has a very different parameterization.

There are two main limitations when our parameterization of the turbulent regime is applied to the Earth secondary convection beneath the lithosphere. First, plate tectonics is not taken into account in this work. However, *Doin et al.* [1997] imposed velocities at the surface of a convecting box in order to mimic plate tectonics. As shown previously, the heat transfer through the continental lithosphere in their experiments fits our relationship in the turbulent regime well. Therefore this relationship describes accurately the intensity of secondary convection. Second, our simulations do not include internal heat generation, the geometry of the mantle flow at large depth, that is, the physics of the material flow across the 670 km discontinuity, nor the Earth's curvature. Then, if the Earth's convection is layered, it is more appropriate to scale our results to the upper mantle. However, the surface heat flow, obtained when equations (9), (11), and (15) are dimensionalized, depends on local parameters at the base of the UTBL, such as the effective viscosity and rheology, but does not depend on the height of the convective layer. Therefore our law should be valid whatever the geometry of the convective flow at depth.

The studies of *Grasset and Parmentier* [1998], with a fluid heated from within, or *Davaille and Jaupart* [1993], with transient cooling experiments, yield parameterization in the turbulent regime very similar to ours ($Nu = 0.47Ra^{1/3}b_{\text{eff}}^{-4/3}$ versus $Nu = 0.52Ra^{1/3}b_{\text{eff}}^{-4/3}$). The difference between our simulations and theirs is the presence (or absence, respectively) of a lower thermal boundary layer and therefore of a large-scale flow. We believe that on the Earth there is interaction between at least two scales of convection. Plate tectonics is the expression of a large-scale convection in the mantle. Although the latter has a different nature than the large-scale flow present in our experiments, it also introduces a shearing of thermal boundary layers and should also carry away small-scale instabilities. Moreover, the presence of hot spots associated with intraplate volcanism

Table 4. Values of the Earth Constants Used to Dimensionalize the Equations

Constant	Symbol	Value
Total temperature drop	ΔT	1800 K
Internal temperature	T_i	1573 K
Thermal conductivity	k	3.1 W m^{-1} K^{-1}
Thermal diffusivity	K	8×10^{-7} m^2 s^{-1}
Thermal expansion coefficient	α	3.5×10^{-5} K^{-1}
Density	ρ	3300 kg m^{-3}
Universal gas constant	R	8.31 J mol^{-1} K^{-1}

suggests that a hot lower thermal boundary layer exists either at the 670 km discontinuity or at the bottom of the mantle. The mechanism of interaction between this hot boundary layer and the lithosphere is still not well known. The relative importance of thermals originating from either the lower thermal boundary layer or the upper thermal boundary layer is not well quantified. However, the influence of plumes might mostly be to feed the asthenosphere with hotter material, therefore decreasing its viscosity and enhancing small-scale convection [*Moore et al.*, 1998; *Yuen and Fleitout*, 1985]. The comparison of this work with those of *Grasset and Parmentier* [1998], *Davaille and Jaupart* [1993], and *Doin et al.* [1997] shows that the interaction between the various scales of convection that may exist in the Earth does not significantly influence the heat transfer through the lithosphere at equilibrium.

Let us now assume that a secondary flow at the base of the oceanic lithosphere is the heat source responsible for the flattening of the seafloor at old ages. One estimates this average heat transfer to about 40 to 50 mW m^{-2} [*Doin and Fleitout*, 1996]. We have shown that this heat transfer is controlled by local parameters and follows the equations established in the turbulent regime. Using a dimensional form of equations (9) and (11), constants listed in Table 4, and extrapolating to an Arrhenius rheology,

$$\dot{\varepsilon} = A^{-1}\sigma^n \exp\left(-\frac{Ea^* + Va^* p}{RT}\right) \qquad (17)$$

we calculate values of the effective viscosity at the base of the lithosphere corresponding to a surface heat flow of 40 to 50 mW/m^2. The results are given in Table 5 for both rheologies and for activation energies (Ea^*) and volumes (Va^*) measured in the laboratory on dry and wet olivine. These values show that with our hypothesis, a zone of low viscosity exists at the base of the lithosphere with a viscosity of the order of 5×10^{18} Pa s. Similar asthenospheric viscosities are reflected by postglacial rebound data away from shield areas and for small ice sheets. Values in the range 10^{18}-10^{20} Pa s are found by *Kaufmann and Wolf* [1996] for the vis-

Table 5. Calculated Viscosities ν and Preexponential Constants A for Newtonian and Non-Newtonian Rheologies and Calculated Strain Rate $\dot{\varepsilon}$ for Non-Newtonian Rheology in the Asthenosphere

	Newtonian Rheology		Non-Newtonian Rheology	
	Dry Olivine	Wet Olivine	Dry Olivine	Wet Olivine
Ea^*, kJ mol^{-1}	300	240	540	430
Va^*, cm^3 mol^{-1}	6	5	15	10
ν_{40}, Pa s	2.8×10^{18}	6.8×10^{18}	7.7×10^{18}	1.6×10^{19}
ν_{50}, Pa s	1.4×10^{18}	3.4×10^{18}	3.2×10^{18}	7.2×10^{18}
$\dot{\varepsilon}_{40}$, s^{-1}	...	...	1.6×10^{-14}	1.1×10^{-14}
$\dot{\varepsilon}_{50}$, s^{-1}	...	...	2.8×10^{-14}	1.9×10^{-14}
A_{1300}, Pa^n s	2.3×10^{7}	7.3×10^{9}	3.1×10^{8}	2.7×10^{13}
A_{1350}, Pa^n s	6.4×10^{7}	1.7×10^{10}	2.1×10^{9}	1.4×10^{14}
A_{Karato}[a], Pa^n s	5.2×10^{10}[b]	1.7×10^{11}[b]	1.3×10^{12}[c]	2.6×10^{14}

Here ν_{40} and ν_{50} ($\dot{\varepsilon}_{40}$ and $\dot{\varepsilon}_{50}$) are calculated for T_i = 1300°C and a surface heat flow of 40 and 50 mW m^{-2}, respectively. A_{1300} and A_{1350} are computed for a heat flow of 50 mW m^{-2}, and an internal temperature of 1300° and 1350°C, respectively.

[a]The preexponential constant is computed from *Karato and Wu* [1993].

[b]A grain size of 1 mm is used.

[c]A shear stress of 10 MPa is used.

cosity of the asthenosphere under the continental margin in the Svalbard Archipelago. Models consistent with the observed rate of uplift and palaeoshorelines in Fennoscandia strongly suggest that the Earth's mantle has a low-viscosity asthenosphere of less of 7.0×10^{19} Pa s [*Fjeldskaar*, 1994], whereas the study of the very fast postglacial rebound in Iceland reveals that the asthenosphere's viscosity beneath Iceland is $1.\times10^{19}$ Pa s or less [*Sigmundsson*, 1991]. Dynamic modeling using geoid, topography, and plate velocity data also favors asthenospheric viscosity comparable to ours (O. Cadek and L. Fleitout, A global geoid model with imposed plate velocities and partial layering, submitted to *Journal of Geophysical Research*, 1999). Conditions in the uppermost mantle may be close to the transition between dislocation creep (non-Newtonian case) and diffusion creep (Newtonian case). For grain sizes greater than 1 mm and stresses greater than 1 MPa, dislocation creep should dominate [*Karato and Wu*, 1993; *Ranalli*, 1991]. In the case of a non-Newtonian rheology, we calculate the value of the strain rate at the base of the lithosphere, using equations (11) and (15). Results for dry and wet olivine, and a surface heat flow of 40 or 50 mW m^{-2}, are given in Table 5. The strain rate due to the secondary convection is not negligible compared to the strain rate due to plate tectonics (roughly estimated as 10^{-14} s^{-1}). We also compute the preexponential constant in the viscosity law A for a surface heat flow of 50 mW m^{-2} and an internal temperature of 1573 or 1623 K. (The internal temperature has more influence on A than the surface heat flow.) The obtained values of A are compared to the values measured in the laboratory (e.g., those listed by *Karato and Wu* [1993]). They compare well with the measured values for wet olivine (in good agreement with *Hirth and Kohlstedt* [1996]), but are 3 orders of magnitude below measured values for dry olivine. However, we have to consider these results with caution because the preexponential constant of viscosity varies a lot with small changes of mantle chemistry. Moreover, the apparent activation energy may depend on the partial pressure of oxygen. Indeed, the power law creep in natural olivine is proportional to $(pO_2)^{1/6}$ [e.g., *Jaoul et al.*, 1980]. Furthermore, *Blundy et al.* [1991] argued that the oxygen fugacity (assimilated to oxygen partial pressure) is buffered by mantle silicate-carbon-fluid equilibria, leading to a strong dependence of $\log(f_{O_2})$ on temperature, that is, $pO_2 \propto \exp(-1.5 \times 10^{-2}T)$. Thus the effective temperature scale is reduced to $\{[2/(n+1)](Ea/RT_i^2)+2.5\times10^{-3}\}^{-1}$ in K. This effect corresponds to an activation energy increase of 80 to 140 kJ mol^{-1} and lowers the predicted viscosity by a factor of 2 or 3.

Acknowledgments. The authors thank P. Tackley, S. Solomatov, U. Christensen, and C. Froidevaux for their useful comments. The research was supported by the contribution 127 to the CNRS-INSU program IT.

References

Blundy, J. D., J. P. Brodholt, and B. J. Wood, Carbon-fluid equilibria and the oxidation state of the upper mantle, *Nature*, *349*, 321–324, 1991.

Booker, J. R., Thermal convection with strongly temperature-dependent viscosity, *J. Fluid Mech.*, *76*, 741–754, 1976.

Castaing, B., G. Gunaratne, F. Heslot, L. Kadanoff, A. Libchaber, S. Thomae, X. Wu, S. Zaleski, and G. Zanetti, Scaling of hard thermal turbulence in Rayleigh-Bénard convection, *J. Fluid Mech.*, *204*, 1–30, 1989.

Christensen, U. R., Convection in a variable-viscosity fluid: Newtonian versus power-law rheology, *Earth Planet. Sci. Lett.*, *64*, 153–162, 1983.

Christensen, U. R., Convection with pressure- and temperature-dependent non-Newtonian rheology, *Geophys. J. R. Astron. Soc.*, *77*, 343–384, 1984a.

Christensen, U. R., Heat transport by variable viscosity convection and implications for the Earth's thermal evolution, *Phys. Earth Planet. Inter.*, *35*, 264–282, 1984b.

Christensen, U. R., Heat transport by variable viscosity convection, II, pressure influence, non-Newtonian rheology and decaying heat sources, *Phys. Earth Planet. Inter.*, *37*, 183–205, 1985.

Christensen, U. R., Mantle rheology, constitution and convection, in *Mantle Convection, Plate Tectonics and Global Dynamics*, edited by W. R. Peltier, pp. 595–655. Gordon and Breach, New York, 1989.

Christensen, U. R., and D. A. Yuen, Time dependent convection with non-Newtonian rheology, *J. Geophys. Res.*, *94*, 814–820, 1989.

Cserepes, L., Numerical studies of non-Newtonian mantle convection, *Phys. Earth Planet. Inter.*, *30*, 49–61, 1982.

Davaille, A., and C. Jaupart, Transient high-Rayleigh-number thermal convection with large viscosity variations, *J. Fluid Mech.*, *253*, 141–166, 1993.

Deschamps, F., Convection de Rayleigh-Bénard à viscosité variable: Applications géophysiques et planétologiques, Ph.D. thesis, 250 pp., Univ. Paris XI, 1997.

Doin, M. P., and L. Fleitout, Thermal evolution of the oceanic lithosphere: An alternative view, *Earth Planet. Sci. Lett.*, *142*, 121–136, 1996.

Doin, M.-P., L. Fleitout, and U. Christensen, Mantle convection and stability of depleted and undepleted continental lithosphere, *J. Geophys. Res.*, *102*, 2771–2787, 1997.

Dropkin, D., and E. Somerscales, Heat transfer by natural convection in liquids confined by two parallel plates which are inclined at various angles with respect to the horizontal, *J. Heat Transfer*, *87*, 77–84, 1965.

Fjeldskaar, W., Viscosity and thickness of the asthenosphere detected from the Fennoscandian uplift, *Earth Planet. Sci. Lett.*, *126*, 399–410, 1994.

Fleitout, L., and D. Yuen, Secondary convection and the growth of oceanic lithosphere, *Phys. Earth Planet. Inter.*, *36*, 181–212, 1984a.

Fleitout, L., and D. Yuen, Steady state convection beneath lithospheric plates with temperature- and pressure-dependent viscosity, *J. Geophys. Res.*, *89*, 9227–9244, 1984b.

Fowler, A. C., Fast thermoviscous convection, *Stud. Appl. Math.*, *72*, 189–219, 1985.

Frick, H., F. H. Busse, and R. M. Clever, Steady three-dimensional convection at high Prandtl numbers, *J. Fluid Mech.*, *127*, 141–153, 1983.

Giannandrea, E., and U. Christensen, Variable viscosity convection experiments with a stress-free upper boundary and implications for the heat transport in the Earth's mantle, *Phys. Earth Planet. Inter.*, *78*, 139–152, 1993.

Goldstein, R. J., H. D. Chiang, and D. L. See, High-Rayleigh number convection in a horizontal enclosure, *J. Fluid Mech.*, *213*, 111–126, 1990.

Grasset, O., and E. M. Parmentier, Thermal convection in a volumetrically heated, infinite Prandtl number fluid with strongly temperature-dependent viscosity. Implications for planetary thermal evolution, *J. Geophys. Res.*, *103*, 18,171–18,181, 1998.

Hansen, U., and A. Ebel, Time-dependent thermal convection – A possible explanation for a multiscale flow in the Earth's mantle, *Geophys. J.*, *94*, 181–191, 1988.

Hansen, U., D. A. Yuen, and S. E. Kroening, Transition to hard turbulence in thermal convection at infinite Prandtl number, *Phys. Fluids*, *A24*, 2157–2163, 1990.

Hansen, U., D. A. Yuen, and A. V. Malevsky, Comparison of steady-state and strongly chaotic thermal convection at high Rayleigh number, *Phys. Rev. A*, *46*, 4742–4754, 1992.

Hirth, G., and D. L. Kohlstedt, Water in the oceanic upper mantle: Implications for rheology, melt extraction and the evolution of the lithosphere, *Earth Planet. Sci. Lett.*, *144*, 93–108, 1996.

Honda, S., Local Rayleigh and Nusselt numbers for Cartesian convection with temperature-dependent viscosity, *Geophys. Res. Lett.*, *23*, 2445–2448, 1996.

Howard, L. N., Convection at high Rayleigh number, in *Proceedings of the 11th International Congress on Applied Mechanics*, edited by H. Gortler, pp. 1109–1115. Springer-Verlag, New York, 1964.

Jaoul, O., C. Froidevaux, W. B. Durham, and M. Michaut, Oxygen self-diffusion in Fosterite: Implications for the high-temperature creep mechanism, *Earth Planet. Sci. Lett.*, *47*, 391–397, 1980.

Jarvis, G. T., Time-dependent convection in the Earth's mantle, *Phys. Earth Planet. Inter.*, *36*, 305–327, 1984.

Jarvis, G. T., and W. R. Peltier, Mantle convection as a boundary layer phenomenon, *Geophys. J. R. Astron. Soc.*, *68*, 389–427, 1982.

Karato, S. I., and P. Wu, Rheology of the upper mantle: A synthesis, *Science*, *260*, 771–778, 1993.

Kaufmann, G., and D. Wolf, Deglacial land emergence and lateral upper-mantle heterogeneity in the Svalbard Archipelago, II, Extended results for high-resolution load models, *Geophys. J. Int.*, *127*, 125–140, 1996.

Kraichnan, R. H., Turbulent thermal convection at arbitrary Prandtl number, *Phys. Fluids*, *5*, 1374–1389, 1962.

Krishnamurti, R., and L. N. Howard, Large-scale flow generation in turbulent convection, *Proc. Natl. Acad. Sci.*, *78*, 1981–1985, 1981.

Lambeck, K., C. Smither, and P. Johnston, Sea-level change, glacial rebound and mantle viscosity for northern Europe, *Geophys. J. Int.*, *134*, 102–144, 1998.

Larsen, T. B., D. A. Yuen, A. V. Malevski, and A. J. Smedsmo, Dynamics of thermal convection with Newtonian temperature-dependent viscosity at high Rayleigh number, *Phys. Earth Planet. Inter.*, *89*, 9–33, 1995.

Larsen, T. B., D. A. Yuen, A. J. Smedsmo, and A. V. Malevski, Generation of fast timescale phenomena in thermo-mechanical processes, *Phys. Earth Planet. Inter.*, *102*, 213–222, 1997.

Moore, W. B., G. Schubert, and P. Tackley, Three-dimensional simulations of plume-lithosphere interaction at the Hawaiian swell, *Science*, *279*, 1008–1011, 1998.

Moresi, L.-N., and V. S. Solomatov, Numerical investigation of 2D convection with extremely large viscosity variations, *Phys. Fluids*, *7*, 2154–2162, 1995.

Morris, S., and D. Canright, A boundary-layer analysis of Bénard convection in a fluid of strongly temperature-dependent viscosity, *Phys. Earth Planet. Inter.*, *36*, 355–373, 1984.

Nataf, H. C., and F. M. Richter, Convection experiments in fluids with highly temperature-dependent viscosity and the thermal evolution of the planets, *Phys. Earth Planet. Inter.*, *29*, 320–329, 1982.

Ogawa, M., G. Schubert, and A. Zebib, Numerical simulations of three-dimensional thermal convection in a fluid with strongly temperature-dependent viscosity, *J. Fluid Mech.*, *233*, 299–328, 1991.

Olson, P., A comparison of heat transfer laws for mantle convection at very high Rayleigh numbers, *Phys. Earth Planet. Inter.*, *48*, 153–160, 1987.

Parmentier, E. M., and J. Morgan, Thermal convection in non-Newtonian fluids: Volumetric heating and boundary layer scaling, *J. Geophys. Res.*, *87*, 7757–7762, 1982.

Parmentier, E. M., D. L. Turcotte, and K. E. Torrance, Studies of finite amplitude non-Newtonian thermal convection with application to convection in the Earth's mantle, *J. Geophys. Res.*, *81*, 1839–1846, 1976.

Parmentier, E. M., C. Sotin, and B. J. Travis, Turbulent 3-D thermal convection in an infinite Prandtl number, volumetrically heated fluid: implications for mantle dynamics, *Geophys. J. Int.*, *116*, 241–251, 1994.

Parsons, B., and J. G. Sclater, An analysis of the variation of ocean floor bathymetry and heat flow with age, *J. Geophys. Res.*, *82*, 803–827, 1977.

Ranalli, G., The microphysical approach to mantle rheology, in *Glacial Isostasy, Sea-Level and Mantle Rheology*, edited by R. Sabadini, K. Lambeck, and E. Boschi, pp. 343–378. Kluwer Acad., Norwell, Mass., 1991.

Ratcliff, J. T., G. Schubert, and A. Zebib, Three-dimensional variable viscosity convection of an infinite Prandtl number Boussinesq fluid in a spherical shell, *Geophys. Res. Lett.*, *22*, 2227–2230, 1995.

Ratcliff, J. T., G. Schubert, and A. Zebib, Steady tetrahedral and cubic patterns of spherical shell convection with temperature-dependent viscosity, *J. Geophys. Res.*, *101*, 25,473–25,484, 1996.

Ratcliff, J. T., P. J. Tackley, G. Schubert, and A. Zebib, Transitions in thermal convection with strongly variable viscosity, *Phys. Earth Planet. Inter.*, *102*, 201–212, 1997.

Reese, C., and V. Solomatov, Heat transport efficiency for stagnant lid convection with dislocation viscosity: Application to Mars and Venus, *J. Geophys. Res.*, *103*, 13,643–13,657, 1998.

Ricard, Y., and C. Vigny, Mantle dynamics with induced plate tectonics, *J. Geophys. Res.*, *94*, 17,543–17,559, 1989.

Roberts, G. O., Fast isoviscous Bénard convection, *Geophys. Astrophys. Fluid Dyn.*, *12*, 235–272, 1979.

Schubert, G., and C. A. Anderson, Finite element calculations of very high Rayleigh number thermal convection, *Geophys. J. R. Astron. Soc.*, *80*, 575–601, 1985.

Sigmundsson, F., Post-glacial rebound and asthenosphere viscosity in Iceland, *Geophys. Res. Lett.*, *18*, 1131–1134, 1991.

Sirovich, L., S. Balachandar, and M. R. Maxey, Simulations of turbulent thermal convection, *Phys. Fluids*, *A12*, 1911–1914, 1989.

Sleep, N. H., Lithospheric thinning by midplate mantle plumes and the thermal history of hot plume material ponded at sublithospheric depths, *J. Geophys. Res.*, *99*, 9327–9343, 1994.

Solomatov, V. S., Scaling of temperature- and stress-dependent viscosity convection, *Phys. Fluids*, *7*, 266–274, 1995.

Solomatov, V. S., and L. N. Moresi, Three regimes of mantle convection with non-Newtonian viscosity and stagnant lid

convection on the terrestrial planets, *Geophys. Res. Lett.*, *24*, 1907–1910, 1997.

Somerscales, E. F. C., and I. W. Gazda, Thermal convection in high Prandtl number liquids at high Rayleigh numbers, Rensselaer Polytech. Inst., *ME Rep. HT-5*. Troy, N. Y., 1968.

Stengel, K. C., D. S. Oliver, and J. R. Booker, Onset of convection in a variable viscosity fluid, *J. Fluid Mech.*, *120*, 411–431, 1982.

Turcotte, D. L., and E. R. Oxburgh, Finite amplitude convective cells and continental drifts, *J. Fluid Mech.*, *28*, 29–42, 1967.

Yuen, D. A., and L. Fleitout, Thinning of the lithosphere by small-scale convective destabilization, *Nature*, *313*, 125–128, 1985.

M. P. Doin, C. Dumoulin, and L. Fleitout, Département de Géophysique, Ecole Normale Supérieure, 24 Rue Lhomond, 75231 Paris Cedex 05, France. (doin@geophy.ens.fr; dumoulin@geophy.ens.fr; fleitout@geophy.ens.fr)

(Received August 24, 1998; revised January 29, 1999; accepted March 3, 1999.)